

GUIDANCE FOR ELLIPTIC ORBIT RENDEZVOUS

Thomas V. Peters,^{*} and Luigi Stripoli,[†]

This paper provides an overview of a guidance function for autonomous elliptic orbit rendezvous. The basic design philosophy is to exploit the similarities between circular orbit rendezvous and elliptic orbit rendezvous to the maximum possible extent. Analogous maneuvers to the Hohmann transfer and the radial impulsive transfer are presented. These maneuvers are incorporated into a comprehensive strategy for the long-range and short-range rendezvous phases respectively. For each rendezvous phase, the guidance strategy is broken down in a set of decision criteria, which uniquely identify the possible situations that may occur during that phase. In turn, each situation is associated with the appropriate response in terms of maneuver type and goal. The implementation of a guidance function using these principles leads to good results for all scenarios and initial conditions that have been identified as applicable.

INTRODUCTION

This paper provides an outline of the guidance algorithms that were created for a simulator of highly autonomous rendezvous operations in elliptical orbits. The main need for a guidance function that can handle rendezvous in elliptical orbits in a highly autonomous mission is the Mars Sample Return. The Mars Sample Return mission consists of (at least) two spacecraft. The first spacecraft lands on Mars, collects samples, and places them in a sample container. Next, the sample container is put into a small launch vehicle, the Mars Ascent Vehicle (MAV), which is launched into a circular orbit. A second spacecraft, the Earth Return Vehicle (ERV) then performs rendezvous operations to retrieve the samples. Two alternative scenarios exist. In the first scenario, the MAV releases the sample in orbit, and the ERV captures the sample container. In the second scenario, the ERV docks to the MAV after which the sample container is transferred from the MAV to the ERV. After the transfer the ERV takes the samples back to Earth. The need for autonomy and robustness stems mainly from the long delays in communication, while the elliptic orbit would serve either as a contingency scenario or as a propellant-saving alternative¹.

During the development of the guidance algorithms, the goal has been to design elliptic orbit rendezvous maneuvers and trajectories that are similar to maneuvers and trajectories for circular orbit rendezvous. This attempt to draw a close parallel between rendezvous maneuvers and trajectories for circular orbits and those for elliptic orbits is motivated by the fact that the dynamics equations for elliptic orbit rendezvous are a generalization of the dynamics equations for circular orbit rendezvous. If such a generalization is successful, elliptic orbit rendezvous strategies could draw from a large body of literature on strategies.

^{*} MSc., AST, GMV, S.A., C. Isaac Newton 11 P.T.M. 28760 Tres Cantos, Madrid, Spain.

[†] MSc., AST, GMV, S.A., C. Isaac Newton 11 P.T.M. 28760 Tres Cantos, Madrid, Spain

To fulfill the need for autonomy, a broad range of rendezvous strategies has been analyzed as a sequence of guidance commands issued at the occurrence of specific values of the relative state vector, and with specific objectives, requirements and constraints. The objective of this analysis has been to derive a concise set of decision criteria for determining the correct guidance command at any given moment. The main inspirations for the overall guidance strategy has been the rendezvous profile of the ATV mission and the Automated Rendezvous Experiment (ARX)^{2,3}.

This paper is divided into several segments. The first segment discusses the notation used to describe the relative motion, and discusses the similarities between elliptic and circular orbit rendezvous. The second segment discusses the core trajectory and maneuver types that were developed and / or defined. The third segment builds on the second segment by placing these elements into a broader overall strategy for rendezvous that is applicable to both circular and elliptic orbits, and the fourth segment discusses some of the results obtained with this guidance function.

NOTATIONS

The relative motion is described using a differential orbital element notation^{4,5}. This notation is partly based on the Yamanaka-Ankersen equations⁶, and can be interpreted as a different factorization or re-parameterization of the state-transition matrix⁷. All differential elements except the differential true anomaly are constant along a trajectory.

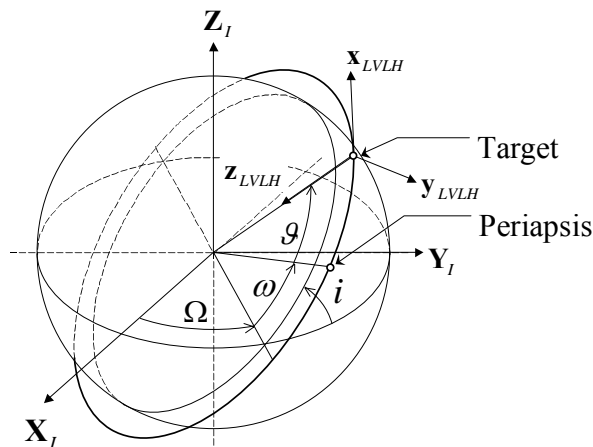


Figure 1. The local vertical, local horizontal frame.

The reference frame used to describe the motion is the local vertical, local horizontal frame. The origin of the reference frame is the target satellite. The z-axis of this reference frame points towards the central body, the y-axis points in the direction opposite to the orbital angular momentum vector and the x-axis completes the right-handed reference frame. The classical Keplerian elements are used to describe the motion of the target spacecraft. The relative state vector of the chaser spacecraft is defined as $\mathbf{x} = [x \ y \ z \ \dot{x} \ \dot{y} \ \dot{z}]^T$. The state at some time 2 can be related to the state at an earlier time 1 by means of the state transition matrix.

$$\mathbf{x}_2 = \Phi_{1 \rightarrow 2} \mathbf{x}_1 \quad (1)$$

where $\Phi_{1 \rightarrow 2}$ denotes the linear state transition matrix. The dynamics of the linearized rendezvous problem are such that the motion in the y-direction is uncoupled from the motion in the or-

bital plane, while the motions in the xz -plane are coupled. The motion can also be described in terms of differences in orbital elements, which are constants of motion for the relative motion of the spacecraft (as well as for the absolute motion). The state transition matrix can be parameterized in terms of differences in orbital elements between the target and the chaser spacecraft. In this case, the state transition matrix becomes the product of three matrices.

$$\Phi_{1 \rightarrow 2} = \mathbf{B}_2 \Phi_{\alpha, 1 \rightarrow 2} \mathbf{B}_1^{-1} \quad (2)$$

where Φ_{α} is the orbital element transition matrix, and \mathbf{B} and its inverse are matrices of partial derivatives that map the differences in orbital elements to the Cartesian state vector and vice-versa. The set of orbital element differences $\Delta \alpha = [\Delta a \ \Delta e \ \Delta i \ \Delta \Omega \ \Delta \omega \ \Delta \mathcal{G}]^T$ provides an alternative description of the motion of the chaser. Orbital element differences have some advantages over the Cartesian description of the motion of the chaser. For example, a coupling exists between the difference in semi-major axis and the difference in true anomaly that produces a secular change in the true anomaly. No other couplings exist that produce secular changes. For this reason, periodic relative trajectories can easily be found by requiring that the difference in semi-major axis remains zero. As shown below, the parallels between elliptic orbit rendezvous and circular orbit rendezvous can be seen more easily by using differences in orbital elements. Orbital element differences also allow a simpler interpretation of the geometry of the problem than the Cartesian state vector. It should be noted, though, that the use of classical Keplerian elements introduces artificial singularities in the solution at zero eccentricity and zero inclination. These singularities are not present if the dynamics equations are solved directly. In addition, the state transition matrix for the orbital elements shows a coupling between the difference in eccentricity and the true anomaly that is periodic in nature. A set of orbital elements that removes the dependence of the fast element on the eccentricity and that uncouples the out-of-plane motion can simplify the state transition matrix⁸, and remove the singularities. In spite of these apparent disadvantages the Keplerian elements are used because they are easy to interpret geometrically, and because problems due to the coupling between the eccentricity and the true anomaly, the coupling of the in-plane and out-of-plane motions and the effect of singularities can easily be circumvented.

As mentioned, a number of similarities exist in the dynamics of circular and elliptic orbit rendezvous that can be exploited when designing rendezvous trajectories, maneuvers and strategies. Yamanaka and Ankersen show that the state transition matrix for elliptic orbits becomes equal to the Clohessy-Wiltshire transition matrix when the eccentricity goes to zero. A comparison of the travelling ellipse formulation⁹ and the formulation of the state transition matrix in terms of orbital elements shows how these similarities can be exploited. For example, the secular drift in the along-track coordinate that is caused by a difference in semi-major axis is 1,5 times the local orbital rate. The center of the travelling ellipse moves along the x -axis with a constant velocity that is equal to 1,5 times the z -coordinate of the center of the ellipse. The difference in true anomaly and the difference in semi-major axis can be associated with the x - and z -coordinates of the center of the travelling ellipse. Likewise, the differences in eccentricity and argument of perigee can be associated with the motion of the chaser around the center of the ellipse. The parameters that describe the travelling ellipse are constants of motion that can be associated with the orbital elements¹⁰. Because of the close analogy, strategies for circular orbit rendezvous can be adapted to elliptic orbit rendezvous. In particular, trajectory diagrams for circular rendezvous using R -bar and V -bar can be used to represent elliptic rendezvous trajectories.

TRAJECTORY DEFINITIONS AND ALGORITHMS

The definition of the rendezvous trajectories and algorithms for elliptic orbit rendezvous closely parallels the definition of said trajectories and algorithms for circular orbit rendezvous.

Trajectories

The flight path angle is the angle between the velocity vector of the target spacecraft expressed in the local vertical, local horizontal frame and the x-axis of the local vertical, local horizontal frame. The flight path angle provides the direction of V-bar.

$$\sin \gamma = \frac{e \sin \mathcal{G}}{\sqrt{2\rho - (1 - e^2)}}, \quad \cos \gamma = \frac{\rho}{\sqrt{2\rho - (1 - e^2)}} \quad (3)$$

where $\rho = 1 + e \cos \mathcal{G}$. Unlike the case of circular rendezvous, in elliptic orbit rendezvous the angle between R-bar and V-bar is not constant, because R-bar is equal to the z-axis in both the circular and the elliptic case. This means that two options exist for defining the reference frame for analyzing the maneuvers and trajectories for elliptic rendezvous; namely, the reference frame can be aligned either with R-bar or with V-bar. For the analysis of trajectories, the local vertical, local horizontal reference frame (i.e., the reference frame aligned with R-bar) is most commonly used.

When the chaser spacecraft is in a periodic trajectory that remains on V-bar at all times, the chaser is said to be in a hold point trajectory. Figure 2 shows V-bar, the flight path angle and a hold point trajectory.

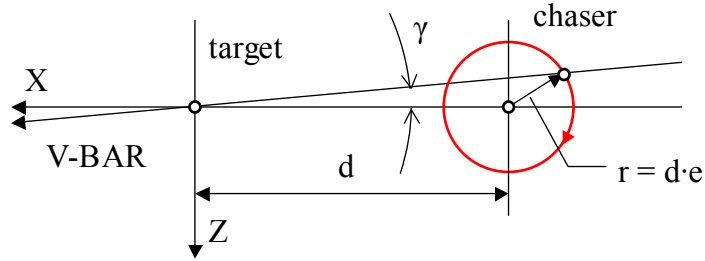


Figure 2. Hold point

The hold point trajectory is a periodic trajectory that is circular, and it is associated with a difference in true anomaly. The distance to the hold point is defined as the distance to the center of the periodic trajectory.

$$\Delta \mathcal{G} = \rho^2 \cdot \frac{d}{p} \quad (4)$$

The hold-point trajectory is the elliptic rendezvous analogy to the hold-point on V-bar. It is used as the start and end of closing maneuvers to the target, as a time-flexible element in the close-range rendezvous strategy.

Another trajectory that is used in the rendezvous strategy is the co-elliptic orbit. In a circular orbit rendezvous scenario, the trajectory is linear, with a constant drift velocity equal to the drift

velocity of the travelling ellipse. In the elliptic case, the condition for co-elliptic orbits¹¹ can be linearized to give:

$$\Delta e = -e \cdot \frac{\Delta a}{a} \quad (5)$$

The co-elliptic drift orbit is then defined by its altitude; the eccentricity difference is given by the equation above, and the difference argument of perigee is zero. Following the definition in reference 11, the differences in inclination and RAAN should be zero as well. For the strategy defined in this paper, the out-of-plane motion is unrestricted.

Finally, a useful check on the trajectory is to establish whether and when a given trajectory crosses V-bar. To derive this criterion, the state vector in the V-bar aligned reference frame is expressed as a function of the differences in orbital elements.

$$\mathbf{x}_{VBAR} = \mathbf{T}_\gamma (\mathbf{B} \cdot \Delta \mathbf{a}) \quad (6)$$

The transformation matrix \mathbf{T}_γ is found from the application of the transport theorem in matrix form¹² and ordering the result in a matrix.

$$\mathbf{T}_\gamma = \begin{bmatrix} \mathbf{R}_\gamma & \mathbf{0} \\ -\boldsymbol{\Omega}_\gamma \mathbf{R}_\gamma & \mathbf{R}_\gamma \end{bmatrix} \quad (7)$$

The rotation matrix \mathbf{R}_γ is a rotation around the y-axis through the flight path angle γ , which can be constructed using the sine and cosine given in equation (3). The angular velocity matrix $\boldsymbol{\Omega}_\gamma$ is the time-derivative of the rotation matrix \mathbf{R}_γ . It is a skew-symmetric angular velocity matrix for the angular velocity around the y-axis, and therefore it requires the time derivative of the flight path angle.

$$\dot{\gamma} = k^2 \rho^2 \frac{\rho - (1 - e^2)}{2\rho - (1 - e^2)} \quad (8)$$

The equation for the z-component from equation (6) needs to be analyzed further. Because the trajectory associated with a difference in true anomaly remains on V-bar (as discussed above), the true anomaly component can be left out. In addition, any non-zero scaling function of a coordinate does not influence the zero crossing of that coordinate. The scaled z-coordinate in the V-bar aligned frame becomes:

$$z_{VBAR}^* = -\rho \frac{\Delta a}{a} + \frac{(1 + e^2) \cos \vartheta + 2e}{1 - e^2} \Delta e + e \sin \vartheta \Delta \omega \quad (9)$$

This expression can be re-written as a trigonometric polynomial as a function of the true anomaly.

$$z_{VBAR}^* = C_1 \sin \vartheta + C_2 \cos \vartheta + C_3 \quad (10)$$

To establish whether a trajectory crosses V-bar, the following can now be formulated.

$$C_1^2 + C_2^2 \geq C_3^2 \quad (11)$$

If this condition holds, the true anomalies at which the crossings occur can be found from:

$$\begin{aligned} \sin \mathcal{G}_1 &= \frac{C_2 C_4 - C_1 C_3}{C_1^2 + C_2^2}, & \cos \mathcal{G}_1 &= -\frac{C_1 C_4 + C_2 C_3}{C_1^2 + C_2^2} \\ \sin \mathcal{G}_2 &= -\frac{C_2 C_4 + C_1 C_3}{C_1^2 + C_2^2}, & \cos \mathcal{G}_2 &= \frac{C_1 C_4 - C_2 C_3}{C_1^2 + C_2^2} \end{aligned} \quad (12)$$

The constants C1 to C4 are given by:

$$\begin{aligned} C_1 &= e\Delta\omega, & C_2 &= \frac{1+e^2}{1-e^2}\Delta e - \frac{e\Delta a}{a} \\ C_3 &= \frac{2e}{1-e^2}\Delta e - \frac{\Delta a}{a}, & C_4 &= \sqrt{(e\Delta\omega)^2 + (\Delta e)^2} \end{aligned} \quad (13)$$

Maneuvers

The maneuvers discussed here are the two main maneuvers used in the rendezvous strategies for ATV and the ARX (see references 2 & 3). Maneuvers are analyzed as pairs of impulsive ΔV 's. A general transfer maneuver between state \mathbf{x}_1 at time 1 and \mathbf{x}_2 at time 2 by means of two impulses $\Delta \mathbf{V}_1$ and $\Delta \mathbf{V}_2$ is given by:

$$\mathbf{x}_2 = \Phi_{1 \rightarrow 2}(\mathbf{x}_1 + \mathbf{G}_1 \Delta \mathbf{V}_1) + \mathbf{G}_2 \Delta \mathbf{V}_2 \quad (14)$$

where the matrix \mathbf{G} is composed of a three by three zero matrix stacked on a three by three identity matrix. The maneuvers described below are derived by placing suitable constraints on equation (14). These constraints can be, amongst others, constraints on the shape of the initial and final trajectories, transfer duration, periodicity, etc. Considering only the in-plane motion, equation (14) consists of four separate equations, while the total number of degrees of freedom is five, namely two per ΔV and one for the transfer time. For each of the maneuvers the burn duration is computed. Times 1 and 2 are considered to be the center of the burn.

The most important maneuver during the long-range rendezvous phase is the cotangential maneuver. The cotangential transfer is close to the optimal transfer between elliptical orbits¹³. For eccentricities smaller than 0.2, the total ΔV required for the cotangential transfer is at most 1% more than the ΔV required for the optimal transfer^{14, 15}. The main purpose of the cotangential transfer is to transfer from an orbit of a certain altitude to an orbit with a different altitude. The cotangential maneuver is a generalization of the Hohmann transfer used in circular orbit rendezvous. The characteristic that is preserved is the orientation of the ΔV ; in both the circular and elliptical case, the ΔV is applied parallel to the target spacecraft velocity vector, or \mathbf{V} -bar¹⁶. The core of the cotangential transfer algorithm computes the required transfer angle and the magnitude of the first and second ΔV . The algorithm can be seen as a linearisation of the algorithms presented in references 13, 14 & 16. First, the differences in orbital element differences are scaled as needed, such that:

$$\Delta a^* = \frac{\Delta a_2 - \Delta a_1}{a}, \quad \Delta e^* = \Delta e_2 - \Delta e_1, \quad \Delta \omega^* = \Delta \omega_2 - \Delta \omega_1 \quad (15)$$

The ΔV 's are scaled and made non-dimensional as follows:

$$\Delta V = \Delta V^* \cdot \frac{1}{2} p k^2 \sqrt{2\rho - (1 - e^2)} \quad (16)$$

where p is the semi-latus rectum and k^2 is equal to:

$$k^2 = \sqrt{\frac{\mu}{p^3}} \quad (17)$$

Note that this scaling factor is variable along the orbit because of the p term that depends on the true anomaly. Three auxiliary constants are computed. The first one is equal to the sum of the two scaled, non-dimensional ΔV 's.

$$\begin{aligned} K_1 &= \Delta V_1^* + \Delta V_2^* = \Delta a^* - \frac{2e}{1-e^2} \Delta e^* \\ K_2 &= e \cdot K_1 - \Delta e^* \\ K_3 &= e \Delta \omega^* \end{aligned} \quad (18)$$

Next, the sine and the cosine of the transfer angle are computed:

$$\sin \varphi = \frac{2P_1 P_2}{P_1^2 + P_2^2}, \quad \cos \varphi = \frac{P_2^2 - P_1^2}{P_1^2 + P_2^2} \quad (19)$$

where $\varphi = \mathcal{G}_2 - \mathcal{G}_1$ is the transfer angle, and the coefficients P_1 and P_2 are defined as:

$$\begin{aligned} P_1 &= K_1 + K_2 \cos \mathcal{G}_1 - K_3 \sin \mathcal{G}_1 \\ P_2 &= K_2 \sin \mathcal{G}_1 + K_3 \cos \mathcal{G}_1 \end{aligned} \quad (20)$$

The scaled, non-dimensional ΔV 's can be computed using:

$$\Delta V_2^* = \frac{P_1^2 + P_2^2}{2P_1}, \quad \Delta V_1^* = K_1 - \Delta V_2^* \quad (21)$$

The most important maneuver type during close range rendezvous is the periodic hop maneuver. The periodic hop is a generalization of the radial impulsive transfer for circular orbit (see, for example, reference 9). The periodic hop maneuver provides a periodic transfer trajectory between two hold points. As defined in equation (4) this means that the initial and final differences in orbital elements consist of differences in true anomaly only. The transfer angle is found from:

$$\sin \varphi = \frac{2Q_1 Q_2}{Q_1^2 + Q_2^2}, \quad \cos \varphi = \frac{Q_2^2 - Q_1^2}{Q_1^2 + Q_2^2} \quad (22)$$

The coefficients Q_1 and Q_2 are defined as:

$$\begin{aligned} Q_1 &= 2e \sin \mathcal{G}_1 \\ Q_2 &= 2\rho_1 - (1 - e^2) \end{aligned} \quad (23)$$

The ΔV 's are scaled according to:

$$\Delta V = \Delta V^* \cdot k^2 \rho \sqrt{2\rho - (1 - e^2)} \quad (24)$$

Now the magnitudes of the velocity impulses can be found from:

$$\Delta V_1^* = \frac{\rho_2^2}{(1 + \rho_1) - (1 + \rho_2) \cos \varphi} \cdot d, \quad \Delta V_2^* = \frac{(1 - \rho_2)(1 + \rho_1) - \cos \varphi}{(1 + \rho_1) - (1 + \rho_2) \cos \varphi} \cdot d \quad (25)$$

where d represents the hop distance. Apart from these two main maneuvers, several other maneuvers are included into the guidance function. These maneuvers are relatively straightforward to compute. These are the two-point transfer (also called the linear Lambert transfer, see reference 9), out-of-plane control, the fly-around, the V-bar crossing stop maneuver and the tangential burn hop maneuver. The two-point transfer maneuver is computed exactly in the same way as in circular orbit rendezvous: using a fixed transfer time, the appropriate portion of the state transition matrix is inverted to compute the required ΔV . This maneuver is used to perform correction maneuvers. The out-of-plane control computes the times at which the chaser crosses the orbital plane and computes the ΔV required to stop the motion. If the magnitude of the out-of-plane motion is too large to be cancelled out during one burn, the ΔV is split in such a way that the chaser performs the maximum possible burn at each subsequent node it encounters. At the last node, the ΔV is exactly as big as needed to remove the out-of-plane component of the motion entirely. The fly-around maneuver is a maneuver parallel to V-bar that exactly removes the semi-major axis difference and that puts the chaser into a periodic orbit. This maneuver is used during the short-range phase. The V-bar crossing stop maneuver computes the ΔV required to enter into a hold-point trajectory. This maneuver is computed by means of equations (4) and (10). First, the time of crossing is computed using equation (10), and next, the magnitude of the ΔV is computed by computing the difference between the predicted state vector, and the state vector associated with a hold-point trajectory at the point of crossing. The tangential burn hop maneuver is a back up for the radial hop maneuver in case propellant runs low (the free drift resulting from a tangential burn can be exploited to drift to the target automatically, and so save hopping maneuvers). The tangential burn hop maneuver takes exactly one orbital period, and it is initiated by a tangential burn that introduces the correct amount of drift. An equal and opposite tangential burn is used to end the transfer (see reference 9).

RENDEZVOUS STRATEGIES AND IMPLEMENTATION

The rendezvous is broken down into three phases, each with its corresponding guidance mode: the long-range mode OSTG (Orbit Synchronization Translational Guidance), the short-range mode INTG (Impulsive Nominal Translational Guidance) and a final forced motion approach FTTG (Forced Terminal Translational Guidance). The strategies for the long-range and the short-range modes will be discussed below. The FTTG will not be considered in this paper, because it is a continuous thrust guidance mode instead of an impulsive guidance mode. The general approach to the design of the guidance algorithms is to construct a decision tree that incorporates all possible configurations of the orbital element difference vector, termed situations, and that presents the correct guidance response to the present situation. At each of the nodes of the tree, a switching criterion is applied to establish which branch to take. Ordering the tree in this way

automatically provides the possibility of introducing a hierarchy in the switching criteria, with the most important or critical criterion at the root of the tree and the least critical at the tips of the branches. The division of the rendezvous sequence in a long-range and a short-range phase allows restricting the types of maneuvers that are available during each phase.

Long-range strategy

The rendezvous starts from an initial condition “far away” from the target. The most common initial condition is some 500 km behind and 50 km below the target. Note that this is not the distance at which the guidance function is activated. The guidance is activated as soon as the navigation converges, and the navigation filters take around one orbital period to converge. This leads to an activation of the guidance at a distance of around 100 km. An analysis of the behavior of the long-range guidance algorithms without navigation or control has shown that the guidance algorithms themselves are accurate up to a distance of about 600 km behind the target, and 80 km below the target.

The first action to take in the long-range scenario is to transfer to a co-elliptic orbit. The sign of the difference in semi-major axis of the co-elliptic orbit should be the same as the sign of the difference in semi-major axis of the initial trajectory. That is, if the chaser was originally below the target, it should transfer to a co-elliptic orbit below the target. A diagram of the long-range guidance strategy after the first maneuver is shown in figure 3. In this diagram, four situations and their appropriate actions are indicated. First, if the chaser is located on V-bar (taking into account a certain margin), the chaser is commanded to perform a cotangential maneuver to a drift orbit that causes the chaser to drift towards the target. This is a high drift orbit in case the chaser is located in front of the target and a low drift orbit if the chaser is located behind the target. Second, if the chaser is in the drift orbit at the appropriate distance from the target to reach the staging area on V-bar, the chaser can transfer to V-bar and the long-range phase ends. Third, if the distance is closer to the target than the distance required for reaching the staging area, the chaser is commanded to do nothing and drift past the target. Fourth, if the distance is larger than the distance required to reach the staging area, and the chaser is drifting away from the target, a cotangential maneuver to the opposite drift orbit is commanded.

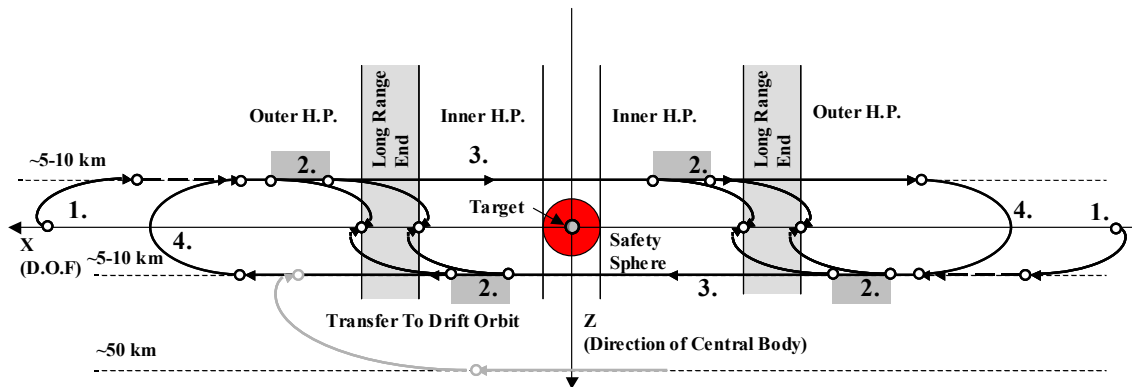


Figure 3. Long-range guidance strategy diagram

In addition to the basic strategy involving cotangential maneuvers, back-up maneuvers and correction maneuvers are available. The quality of the cotangential maneuver is checked by evaluating the transfer angle and the required ΔV . If the transfer angle gets too close to a multiple of one full revolution, or the ΔV becomes too big, the back-up maneuver is used. The correction

maneuver is commanded when the chaser moves outside of a trajectory corridor of a pre-determined size. Both the correction maneuver and the back-up maneuver make use of a two-point transfer or (linear) Lambert algorithm that is based on inverting a partition of the state transition matrix. Lastly, the out-of-plane motion is corrected at the end of the long-range phase.

Table 1 shows the criteria used to determine the current situation during the long-range rendezvous phase. These criteria have a direct impact action (as described in figure 3) that the guidance should take at any given moment. The end condition for the long-range rendezvous is encoded in the current distance and the hold point criteria: if the chaser is located at a hold point between the boundaries of the staging area on V-bar (and no out-of-plane motion is present), the rendezvous phase is completed.

Table 1. Long-range phase criteria.

Criterion	Values		
Semi-major axis difference	big	drift	none
V-bar crossing	yes	no	
Cotangential maneuver OK	yes	no	
Distance after cot. man. to V-bar	outside	between	inside
Drift direction	towards	away	none
Current distance	outside	between	inside
Hold point	yes	no	
Out-of-plane motion	yes	no	

Short-range strategy

The short-range phase starts with the chaser on V-bar, at some distance in front or behind the target. A list of hold points is defined, such that the spacing between the hold points increases as the distance increases. Figure 4 shows the most important situations that may arise, and their appropriate responses. First, the normal situation is to perform a periodic hop maneuver from a hold point at a certain distance to a hold point closer to the target. If the chaser is not located at a hold point, the guidance evaluates between which two hold points it is located. Using a threshold value, the guidance then decides either to move to the closest of the two hold points identified, or to a hold point that is even closer. This evaluation is performed to avoid periodic hops of a very small distance. Second, if the chaser is not in a hold point, close to crossing V-bar at the end of a maneuver and no drift is present, a maneuver is commanded to put the chaser in a hold point trajectory when it crosses V-bar. This maneuver is based on the crossing criterion of equation (12). Third, if a difference in semi-major axis is detected, a tangential maneuver is commanded that negates this difference. Fourth, if the chaser is not performing a periodic hop maneuver and it is not at a hold point, the chaser is commanded to wait for the V-bar crossing closest to the target and perform a maneuver to put the chaser in a hold point trajectory. This is a variation on the second point. Fifth, when the chaser is located at the last hold point in the list, a two-point transfer maneuver is commanded to bring the chaser to the terminal approach point (TAP). At this point, the short-range impulsive guidance mode ends, and forced motion begins.

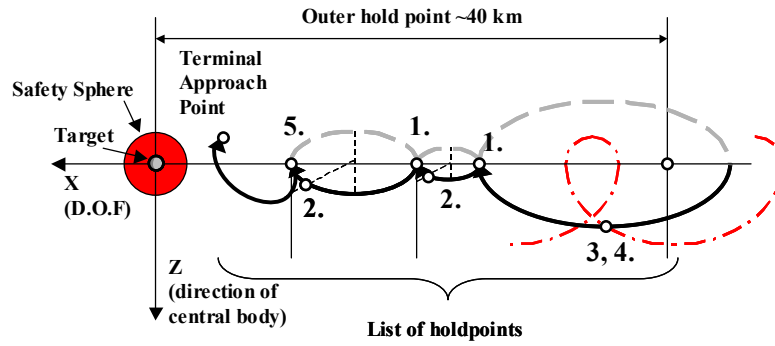


Figure 4. Short-range guidance strategy diagram

Table 2 lists the decision criteria for the short-range rendezvous phase. The first criterion “close to V-BAR crossing” determines when the chaser is close to crossing V-bar and as such provides the cue to prepare the maneuver to enter into a hold point. The “Close to TAP” condition becomes relevant only when the chaser is performing the transfer to the terminal approach point. These two conditions are examples of the dependence of the guidance decision on the current maneuver in progress. All subsequent conditions apply more directly to a situation where the guidance is not currently executing any maneuver. The TAP condition provides the end condition for the short-range guidance phase. This condition is given a high priority, since the guidance would not have to provide any further impulsive maneuvers if the chaser is already at the terminal approach point. The drift condition leads to the third situation identified in figure 4. During the short-range phase, drift is considered undesirable, so this condition is given a high priority. As soon as drift is detected, the guidance will try to correct it. Next, is the criterion that checks whether the chaser is in a hold point. If it is not, the guidance commands a maneuver to enter into a hold point at the next V-bar crossing. This sequence of commands is associated with the situations labeled 3 and 4 in figure 4. The V-bar crossing maneuver is the same type of maneuver commanded at the end of a periodic hop maneuver. If the chaser is in a hold point, the guidance uses the out-of-plane motion criterion to determine whether to control the out-of-plane motion, or to perform a periodic hop to the next hold point in the list. Finally, if the chaser is in a hold point on V-bar sufficiently close to the last hold point, and no out-of-plane motion is present, the maneuver to the terminal approach point is commanded.

Table 2. Short-range phase criteria.

Criterion	Values	
Close to VBAR crossing	yes	no
Close to TAP	yes	no
TAP	yes	no
Drift	yes	no
Hold point	yes	no
Out-of-plane motion	yes	no
Sufficiently close to last hold point	yes	no

Guidance architecture

The guidance function (that is, the maneuver algorithms and higher-level guidance strategy) has been implemented within a broader real-time simulation framework that incorporates other on-board functions such as navigation and control, and mission management, as well as a detailed real-world model. Within this framework, the guidance function is under the control of a mission manager function, that manages the overall mission plan. The mission manager commands, for example, the transition between long-range rendezvous and short-range rendezvous. The real-world model includes sensor and actuator models, and detailed perturbations and actuators models.

The interaction between the guidance and the navigation has been largely omitted from this paper, although it is a very important aspect of the design of the guidance function. The navigation accuracy necessitates the inclusion of correction maneuvers, but also of margins in each of the switching criteria. In addition, the reference orbit of the target that is provided by the navigation needs to be replaced by a Keplerian orbit, because the state transition matrix depends on the validity of Kepler's equation. None of these aspects are treated in the present paper in any level of detail. It should be kept in mind that all the diagrams that follow are simplified specifically with regards to this influence of the navigation.

The guidance function itself has been split into a guidance manager and a guidance library. Figure 5 shows the high-level layout of the guidance function. The guidance library contains all the algorithms for calculating maneuvers (their required ΔV and transfer angle), while the guidance manager contains the decision algorithms needed for the rendezvous strategy. The guidance manager itself contains two major sub-functions, the state prediction and the algorithm scheduler. The state prediction provides the correct input for the computation of maneuvers, such as the time at which a maneuver should start, the desired final state, estimates of the burn durations and any other parameters that may be required in the maneuver computation. The algorithm scheduler implements the guidance strategies described in the preceding section. The state assessment evaluates the criteria listed in table 1 and table 2. The maneuver type decision establishes which maneuver should be applied, and what the goal of the maneuver should be, based on the values of this evaluation of the criteria.

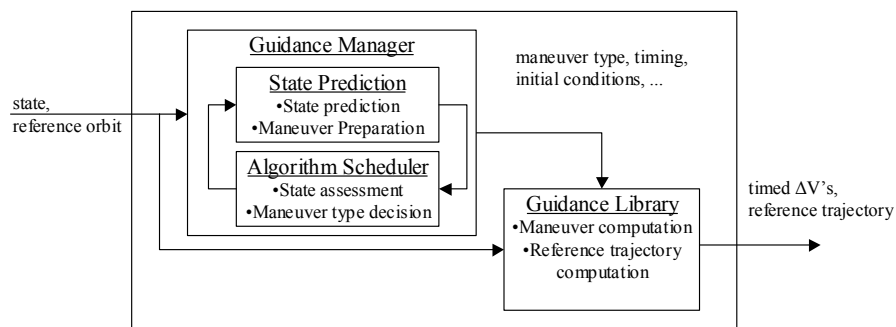


Figure 5. Simplified architecture of the guidance function

The state prediction keeps track of the maneuvers by following the scheme outlined in figure 6. A complete maneuver consists of a set of two (or, in some cases one) ΔV 's plus their associated times of application. The application times are referenced to a time t_0 , which is reset whenever a new maneuver is required. The ΔV 's themselves are characterized by two moments in time, the start of the burn, t'_1 or t'_2 , and the center of the burn t_1 or t_2 , which is the time at which

an impulsive ΔV should be applied. Three reference trajectories are established (this definition also holds for the reference trajectory generation in the guidance library): the first is the trajectory before the application of any maneuvers that is referenced to t_0 and that is valid between t_0 and t'_1 . The second is the trajectory that is valid between the end of the first ΔV and the start of the second ΔV , and that is referenced to time t_1 . Finally, the third reference trajectory is valid after the end of the second ΔV and is referenced to the center of the second burn, t_2 . The reference trajectory between the first and second ΔV is used to determine the need for correction maneuvers.

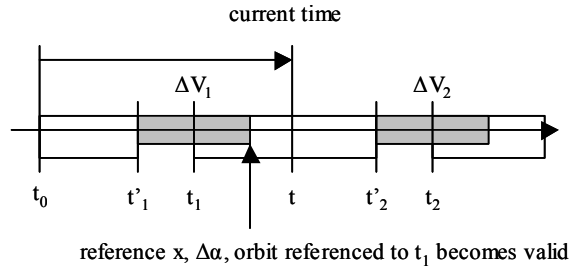


Figure 6. Definition of maneuvers within the guidance manager

The algorithm scheduler contains a module that drives the guidance manager. When a new maneuver is commanded (by the mission manager), the algorithm scheduler starts the process depicted in figure 7.

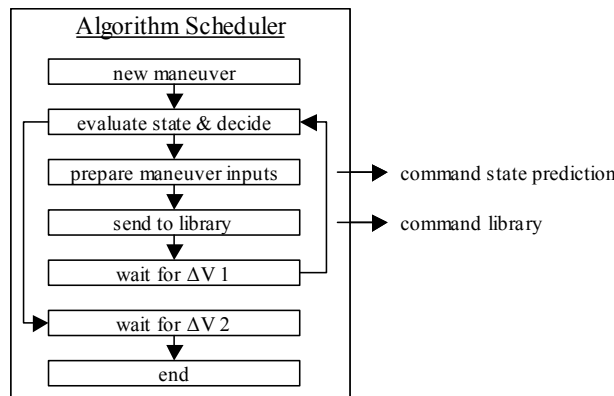


Figure 7. Simplified maneuver planning in the guidance manager

The first step is to evaluate the criteria, and to select the appropriate maneuver type and objective. This information is passed to the state prediction, and the maneuver is prepared. The state prediction now prepares the required inputs for the maneuver algorithms, such as, for example, the state vector at the start and end of the maneuver. In the next step, the maneuver inputs are passed to the library, and the library computes the appropriate ΔV 's and transfer angles. Now the algorithm scheduler waits until the first maneuver is applied, and returns to evaluating the maneuver selection criteria. At this point, the algorithm scheduler mainly checks whether a correction maneuver is required, by comparing the current state vector with the reference state vector. If a correction maneuver is required, it is treated in the same way as a regular maneuver. Otherwise,

the algorithm scheduler waits for the application of the second maneuver, and the process can start again.

SIMULATIONS

An extensive simulation campaign has been carried out for rendezvous in circular and elliptical orbits, around both Earth and Mars. The model mission for the Martian rendezvous is the Mars Sample Return. The target spacecraft is assumed to be a spherical container studded with LIDAR retro-reflectors and an RF beacon. The chaser spacecraft is equipped with an RF sensor, a narrow-angle camera and a LIDAR. Here, one of the simulations for the elliptic rendezvous case will be discussed. Table 3 shows the orbital elements of the target orbit.

Table 3. Orbital elements for MSR elliptic scenario.

Orbital element	Value
Semi-major axis	4643 km
Eccentricity	0.2044
Inclination	115°
RAAN	323.4°
Argument of perigee	0°
True anomaly	0°

The rendezvous scenario is defined as follows. The chaser spacecraft waits in an orbit below the intended target orbit, defined by the parameters given in table 4. The target spacecraft is launched into orbit, and the chaser spacecraft starts searching for the target. After detecting the target's RF beacon, the chaser starts scanning the region of the sky where the signal has been detected. Once both the RF system and the camera have acquired the target and the navigation filter has converged, the guidance is activated. From that point on, the guidance function performs the strategy outlined in the sections above.

Table 4. Initial orbital elements differences for MSR elliptic scenario.

Orbital element difference	Value
Semi-major axis	-50 km
Eccentricity	0.003
Inclination	0.3°
RAAN	0.3°
Argument of perigee	0.3°
True anomaly	-8°

Figure 8 shows the results of the simulation for this particular case. At a distance of about 80 km behind the target and 50 km below the target, the navigation converges and the guidance function is engaged. The first maneuver is a cotangential maneuver to a low drift orbit that ends at about 90 km in front of the target. The drift orbit is a co-elliptic orbit with a semi-major axis dif-

ference of 10 km. Next, the chaser performs a cotangential transfer to the high drift orbit and starts drifting backwards towards the target. At a distance of about 60 km, the chaser initiates a cotangential transfer to V-bar. At that point, the out-of-plane motion is corrected (in the lower half of the figure) and the long-range phase ends.

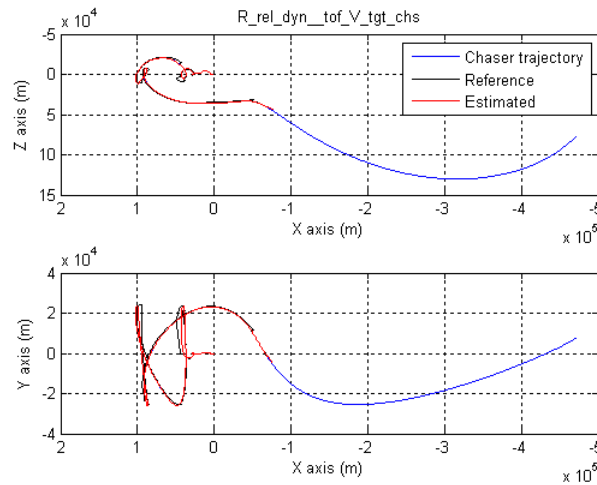


Figure 8. Simulated MSR eccentric orbit rendezvous trajectory

The short-range phase starts at around 40 km from the target. The hold points are located at 50 km, 20 km, 10 km, 5 km, 2 km, 1 km, 500 m, and 200 m. Figure 9 shows a close-up of the close-range rendezvous phase up to capture. The four hold points shown in the figure are located at 2000 meters, 1000 meters, 500 meters and 200 meters, while the terminal approach point is located at +100 meters on the x-axis. Correction maneuvers are visible where a jump occurs in the reference trajectory. At these points, the reference trajectory is reset to the estimated trajectory. At the 2 km hold point, the chaser performs a correction of the out-of-plane motion. The rest of the hop maneuvers show a number of correction maneuvers, but are otherwise uneventful. The rendezvous is completed successfully.

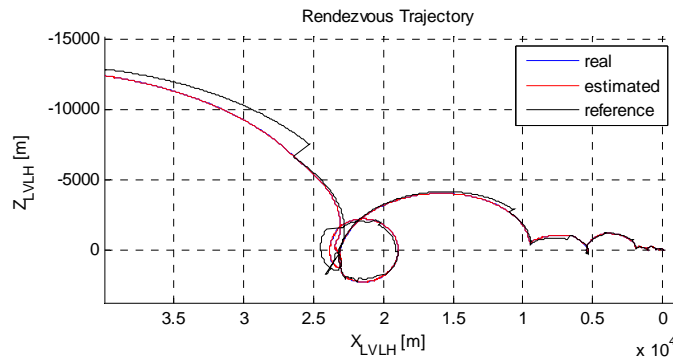


Figure 9. Simulated MSR short-range eccentric orbit rendezvous trajectory

Figure 10 shows a rendezvous trajectory for rendezvous in a circular orbit. In this case, the reference orbit is a 500 km altitude circular orbit, with the same orientation as the orbit listed in

table 3. Here, the rendezvous trajectory displays the general pattern that is present in the elliptic scenario: an initial transfer to a low drift orbit, followed by a transfer to the high drift orbit. In this case, both the initial cotangential transfer and the drift segment towards the target are substantially longer. At About 50 km distance in front of the target, the chaser transfers to V-bar and performs the hopping towards the target.

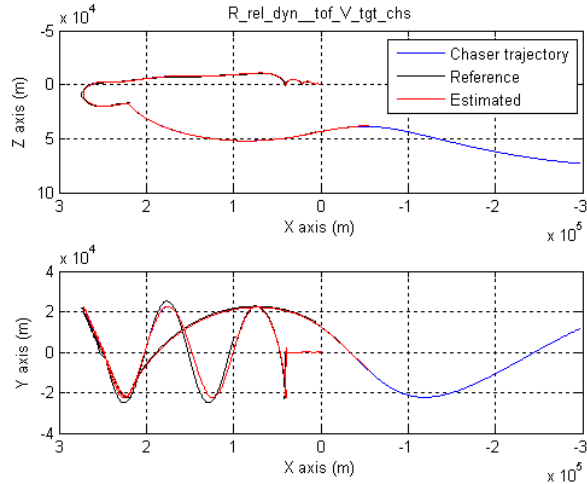


Figure 10. Simulated MSR circular orbit rendezvous trajectory

Many such simulations have been carried out for a broad range of initial conditions, and a broad range of mission parameters (e.g., sensor noise & bias). In all cases, the guidance function has provided the correct rendezvous strategy and rendezvous has successfully been completed. Figure 11 provides an example of the robustness of the rendezvous algorithms to uncertainties in the navigation. These uncertainties are the result of unknown bias and noise in the sensors, and errors in the actuators.

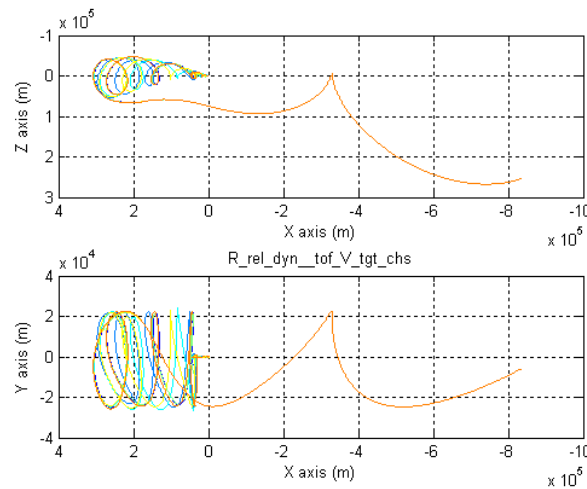


Figure 11. MSR elliptic orbit rendezvous trajectory with varying navigation performance

Similar simulations have been carried out for the variation of initial conditions, and the characteristics of the control system, and all these simulations have been carried out both for circular and elliptical scenarios. In all these cases, the guidance has correctly (and autonomously) provided the correct sequence of maneuvers and the correct reference trajectory.

CONCLUSION

This paper has outlined the development of the guidance function for a detailed rendezvous simulator that can handle rendezvous in both circular and elliptic orbits with a high degree of autonomy. To achieve this goal a comprehensive rendezvous strategy has been developed that consists of a long-range and a short-range phase. The cotangential transfer is the key maneuver for the long-range phase, while the periodic hop maneuver is the most important maneuver for the short-range phase. The algorithms for both maneuvers plus other basic trajectory elements and algorithms have been described, and each of these building blocks has been fitted into the overall rendezvous strategy. It has been explained how the overall strategy has been implemented through a discussion of the architecture of the guidance function. Finally, a brief discussion of the results of simulations carried out with the full simulator has shown that the guidance function is capable of generating a rendezvous profile that leads to successful capture of the target spacecraft.

APPENDIX: STATE TRANSITION MATRIX COMPONENTS

This section describes the state transition matrix factored in terms of Keplerian orbital element differences. The matrix that transforms the differences in orbital elements to a Cartesian state vector is formed by six column vectors, each associated with one of the orbital elements.

$$\mathbf{B} = [\mathbf{b}_a \quad \mathbf{b}_e \quad \mathbf{b}_i \quad \mathbf{b}_\Omega \quad \mathbf{b}_\omega \quad \mathbf{b}_g] \quad (26)$$

The column vectors associated with the orbital elements are given by:

$$\begin{aligned} \mathbf{b}_a &= p\rho^{-1}a^{-1} \begin{bmatrix} 0 & 0 & 1 & \frac{3}{2}k^2\rho^2 & 0 & -\frac{1}{2}k^2es \end{bmatrix}^T \\ \mathbf{b}_e &= a \begin{bmatrix} 0 & 0 & \rho^{-2}((1+e^2)\cos\mathcal{G}+2e) & k^2(3e+(2+e^2)\cos\mathcal{G}) & 0 & -k^2\sin\mathcal{G} \end{bmatrix}^T \\ \mathbf{b}_i &= p\rho^{-1} \begin{bmatrix} 0 & \sin(\omega+\mathcal{G}) & 0 & 0 & k^2(es\sin(\omega+\mathcal{G})+\rho^2\cos(\omega+\mathcal{G})) & 0 \end{bmatrix}^T \\ \mathbf{b}_\Omega &= p\rho^{-1}\sin i \begin{bmatrix} 0 & \cos(\omega+\mathcal{G}) & 0 & 0 & k^2(es\cos(\omega+\mathcal{G})-\rho^2\sin(\omega+\mathcal{G})) & 0 \end{bmatrix}^T + \\ &\quad \mathbf{b}_\omega \cdot \cos i \\ \mathbf{b}_\omega &= p\rho^{-1} \begin{bmatrix} 1 & 0 & 0 & k^2es & 0 & 0 \end{bmatrix}^T \\ \mathbf{b}_g &= p\rho^{-1} \begin{bmatrix} 1 & 0 & -\rho^{-2}es & -k^2es & 0 & k^2(\rho-\rho^2) \end{bmatrix}^T \end{aligned} \quad (27)$$

The inverse of this matrix relates the Cartesian state vector to differences in orbital elements. In this case, each of the rows of the matrix is associated with one of the orbital elements.

$$\mathbf{B}^{-1} = [\mathbf{b}_a^{-1} \quad \mathbf{b}_e^{-1} \quad \mathbf{b}_i^{-1} \quad \mathbf{b}_\Omega^{-1} \quad \mathbf{b}_\omega^{-1} \quad \mathbf{b}_g^{-1}]^T \quad (28)$$

The row vectors of this matrix are given by:

$$\begin{aligned}
\mathbf{b}_a^{-1} &= 2ap^{-2}\rho[-es \ 0 \ -(\rho+\rho^2) \ k^{-2} \ 0 \ -k^{-2}\rho^{-2}es] \\
\mathbf{b}_e^{-1} &= e^{-1}p^{-1}\rho \cdot \\
&\quad [es(\rho^{-2}(1-e^2)-1) \ 0 \ -(\rho+\rho^2-2(1-e^2)) \ k^{-2}\rho^{-2}(\rho^2-(1-e^2)) \ 0 \ -k^{-2}\rho^{-2}es] \\
\mathbf{b}_i^{-1} &= p^{-1}\rho[0 \ \rho^{-2}es\cos(\omega+\vartheta)-\sin(\omega+\vartheta) \ 0 \ 0 \ k^{-2}\rho^{-2}\cos(\omega+\vartheta) \ 0] \\
\mathbf{b}_\Omega^{-1} &= p^{-1}\rho(\sin i)^{-1}[0 \ (\rho^{-2}es\sin(\omega+\vartheta)+\cos(\omega+\vartheta)) \ 0 \ 0 \ -k^{-2}\rho^{-2}\sin(\omega+\vartheta) \ 0] \\
\mathbf{b}_\omega^{-1} &= e^{-1}p^{-1}\rho[e^{-1}(ce-1-\rho^{-1}(1-e^2)) \ 0 \ -\sin\vartheta(2+\rho) \ k^{-2}\rho^{-2}\sin\vartheta(1+\rho) \ 0 \ k^{-2}\rho^{-2}c] \\
&\quad -\mathbf{b}_\Omega^{-1} \cdot \cos i \\
\mathbf{b}_\vartheta^{-1} &= e^{-1}p^{-1}\rho[e\sin^2\vartheta\rho^{-1}(1+\rho) \ 0 \ -\sin\vartheta(2+\rho) \ -k^{-2}\rho^{-2}\sin\vartheta(1+\rho) \ 0 \ -k^{-2}\rho^{-2}c]
\end{aligned} \tag{29}$$

Since the orbit is Keplerian, all of the orbital elements differences are constant, except for the true anomaly. The matrix of partial derivatives of the orbital element differences, or orbital element transition matrix is given by:

$$\Phi_{\alpha,1 \rightarrow 2} = \begin{bmatrix} 1 & 0 & 0 & 0 & 0 & 0 \\ 0 & 1 & 0 & 0 & 0 & 0 \\ 0 & 0 & 1 & 0 & 0 & 0 \\ 0 & 0 & 0 & 1 & 0 & 0 \\ 0 & 0 & 0 & 0 & 1 & 0 \\ \frac{\partial \mathcal{G}(t_2)}{\partial a(t_1)} & \frac{\partial \mathcal{G}(t_2)}{\partial e(t_1)} & 0 & 0 & 0 & \frac{\partial \mathcal{G}(t_2)}{\partial \mathcal{G}(t_1)} \end{bmatrix} \tag{30}$$

The partial derivatives appearing in this matrix that are not zero or one are the partial derivatives to the semi-major axis, the eccentricity and the true anomaly.

$$\begin{aligned}
\frac{\partial \mathcal{G}(t_2)}{\partial a(t_1)} &= -\frac{3}{2} \frac{k^2 \rho_2^2}{a} (t_2 - t_1) = -\frac{3}{2} \frac{\rho_2^2}{a} J \\
\frac{\partial \mathcal{G}(t_2)}{\partial e(t_1)} &= \frac{1}{1-e^2} \left((1+\rho_2)\sin\vartheta_2 - \left(\frac{\rho_2}{\rho_1}\right)^2 (1+\rho_1)\sin\vartheta_1 \right) \\
\frac{\partial \mathcal{G}(t_2)}{\partial \mathcal{G}(t_1)} &= \left(\frac{\rho_2}{\rho_1}\right)^2
\end{aligned} \tag{31}$$

REFERENCES

- ¹ Peters, T. V., "Alternative scenario for Mars Sample Return rendezvous", presentation at the European Workshop on Space Mission Analysis 10-12 December 2007
- ² Fabrega, J., Frezet, M., Gonnaud J.-L. 1997, "ATV GNC during rendezvous", Proceedings Third International Conference on Spacecraft Guidance, Navigation and Control Systems, ESTEC, Noordwijk, The Netherlands, 26-29 November 1996, ESA SP-381 (February 1997)
- ³ Kornfeld, R.P., *et al.* 2003, "New Millennium ST6 Autonomous Rendezvous Experiment (ARX)", Aerospace Conference, Proceedings. 2003 IEEE, Volume 1, Issue , March 8-15, 2003 Page(s): 1 - 380 vol.1, DOI 10.1109/AERO.2003.1235067

- ⁴ Alfriend, K.T. and Schaub, H. 2000, "Hybrid Cartesian and Orbit Element Feedback Law For Formation Flying Spacecraft," Paper No. AIAA 2000-4131, presented at the AIAA Astrodynamics Specialist Conference, Denver, Co
- ⁵ Gim D.-W. & Alfriend K. T. 2003, "State transition matrix of relative motion for the perturbed noncircular reference orbit", *Journal of Guidance, Control and Dynamics*, Vol. 26, No. 6, Nov-Dec 2003, pp 956-971
- ⁶ Yamanaka, K. & Ankersen, F. 2002, "New State Transition Matrix for Relative Motion on an Arbitrary Elliptical Orbit", *Journal of Guidance, Control and Dynamics*, Vol. 25, No. 1, pp. 60-66
- ⁷ D'Amico, S., and Montenbruck, O., "Proximity Operations of Formation-Flying Spacecraft Using an Eccentricity/Inclination Vector Separation," *Journal of Guidance, Control, and Dynamics*, Vol. 29, No. 3, May-June 2006, pp. 554-563.
- ⁸ Montenbruck, O. & Gill, E., 2000, "Satellite Orbits – Models, Methods, and Applications", Springer-Verlag, Berlin Heidelberg
- ⁹ Fehse W., 2003, "Automated Rendezvous and Docking of Spacecraft", Cambridge University Press, Cambridge (UK)
- ¹⁰ D'Amico, S., "Relative Orbital Elements as Integration Constants of the Hill's Equations," DLR, TN 05-08, Cologne, Germany, 2005.
- ¹¹ Whipple, P. H., 1970, "Some Characteristics of Coelliptic Orbits", NASA-CR-109655, Bellcomm, Inc., Washington D.C.
- ¹² Schaub, H & Junkins, J. L. 2003, "Analytical Mechanics of Space Systems", AIAA, Reston, VA
- ¹³ Bender, D. F., 1962, "Optimum Coplanar Two-Impulse Transfers Between Elliptic Orbits", *Aerospace Engineering*, 21, pp. 44-52
- ¹⁴ Moyer, H. G. 1967, "An analytic treatment of cotangential transfer", *AIAA Journal*, 0001-1452, vol.5, no.6, pp. 1197-1198, doi: 10.2514/3.4164
- ¹⁵ Doll, J. R. & Gobetz 1969, F. W., "A survey of impulsive trajectories", *AIAA Journal*, 0001-1452, vol.7, no.5, pp. 801-834, doi: 10.2514/3.5231
- ¹⁶ Vinh, N. X. 1964, "A property of cotangential elliptical transfer orbits", *AIAA Journal*, 0001-1452, vol.2, no.10, pp. 1841-1844, doi: 10.2514/3.2686